ORIGINAL ARTICLE

Validation of a clinical finite element model of the human lumbosacral spine

Yabo Guan · Narayan Yoganandan ·
Jiangyue Zhang · Frank A. Pintar · Joesph F. Cusick ·
Christopher E. Wolfla · Dennis J. Maiman

Abstract Very few finite element models on the lumbosacral spine have been reported because of its unique biomechanical characteristics. In addition, most of these lumbosacral spine models have been only validated with rotation at single moment values, ignoring the inherent nonlinear nature of the moment–rotation response of the spine. Because a majority of lumbar spine surgeries are performed between L4 and S1 levels, and the confidence in the stress analysis output depends on the model validation, the objective of the present study was to develop a unique finite element model of the lumbosacral junction. The clinically applicable model was validated throughout the entire nonlinear range. It was developed using computed tomography scans, subjected to flexion and extension, and left and right lateral bending loads, and quantitatively validated with cumulative variance analyses. Validation results for each loading mode and for each motion segment (L4-L5, L5-S1) and bisegment (L4-S1) are presented in the paper.

Y. Guan · N. Yoganandan (✉) · J. Zhang · F. A. Pintar ·
J. F. Cusick · C. E. Wolfla · D. J. Maiman
Departments of Neurosurgery,
Medical College of Wisconsin,
9200 West Wisconsin Avenue,
Milwaukee, WI 53226, USA
e-mail: yoga@mcw.edu

Y. Guan · N. Yoganandan · J. Zhang ·
F. A. Pintar · D. J. Maiman
VA Medical Center, Milwaukee, WI, USA

1 Introduction

It is well known that the human spine responds nonlinearly to external loads. Computational methods have been used to better understand mechanisms of load transfer in the spine. In particular, finite element models have been developed to investigate the mechanical behavior of the lumbar spine under physiologic and traumatic loads. Many models are focused on the middle or superior lumbar segments [3, 12–14, 19, 27, 28, 30, 33, 34, 37–41, 50, 51]. In contrast, few finite element models have been reported on the lumbosacral spine ([2] for L5–S1; [20] for L4–S1; [31, 32] for L1–S1), a region of greater interest to clinicians. As described below, majority of these lumbosacral models have not used experimentally derived data encompassing the entire nonlinear responses to compare and validate finite element outputs. Validation is a critical step in finite element analysis because confidence in the stress analysis output depends on validation.

Shirazi-Adl and Parnianpour [32] reported results from an L1–S1 finite element model of the lumbar spine under axial compressive loading. In a later study [31], Shirazi-Adl described its biomechanics under flexion–extension and lateral bending at moments up to 15 Nm. Predicted rotation results from the finite element model were compared with experimental data obtained at specific moment magnitudes: 3 Nm moment [11], and 10 Nm moment [23, 44]. More recently, a finite element model of the L4–S1 segment [20] was developed and validated by comparing rotation at single moment value, i.e., 10 Nm under flexion–extension, lateral bending, and torsion, with experimental results [24]. Charriere et al. [2] developed a finite element model of the L5–S1 motion segment

and validated with experimental data from thoracic specimens.

These literature analyses indicate that, while some finite element models include the lower lumbosacral spine, they are not consistent in spinal levels, components, loading, and validation procedures. In addition, validation has been primarily limited to comparing motions at specific moment values, often at the highest magnitude reported by the experiment [22, 29, 36]. Validation at a specific moment value ignores the inherent nonlinear nature of the moment–rotation response of the spine. In order to better validate the model, it is necessary to compare finite element model responses with experimentally obtained results in the whole range, i.e., moving from single point validation to entire curve validation. This is the purpose of the present study.

From a clinical perspective, the vast majority of surgical procedures for physiologic-related spinal disorders are done between L4–5 and L5–S1 levels [4, 16, 35]. This includes intervertebral disc herniation, spondylolisthesis, and facet disease. As indicated above, very few finite element models focusing on these specific segments have been developed, validated, and exercised to study the intrinsic biomechanics of the low back. Consequently, the objective of the present study was to develop and validate (throughout the entire nonlinear range) a clinically applicable nonlinear finite element model of the L4–S1 region of the human vertebral column.

2 Methods

2.1 Geometry

Geometrical details of the human lumbosacral spine (L4–S1) were obtained from high-resolution computed tomography (CT) images of a 37-year old human cadaver in the axial, sagittal, and coronal planes. Digital CT data were imported to a software (Mimics, Materialise Inc., Leuven, Belgium), and three-dimensional geometrical surface of the lumbosacral spine was generated. The exported IGES files from the Mimics software were inputted to TrueGrid pre-processor software (XYZ Scientific Applications, Inc., Livermore, CA, USA) to create hexahedral finite element mesh. Because the geometry of the model was obtained from a spine specimen, geometrical parameters of the vertebrae were evaluated. Specifically, the anteroposterior depth, lateral width, transverse process length, and posterior component dimensions were compared with literature.

The model (Fig. 1) consisted of 4,436 finite elements. Three-dimensional isotropic eight-node solid elements were used for modeling the cancellous core, posterior bony parts of the vertebrae, annulus fibrosis, and nucleus of intervertebral discs. Cortical shell and endplates of the vertebrae were modeled as thin shell elements. Anterior longitudinal ligament, posterior longitudinal ligament, intertransverse ligament, ligamentum flavum, capsular ligament, interspinous ligament, and supraspinous ligament were modeled using tension-only spring elements. Three-dimensional surface-to-surface contact was used to simulate the interaction between the articulating surfaces of facet joints. The initial gap between the articulating surfaces was based on CT images.

2.2 Material properties

The annulus fibrosis of the intervertebral disc was assumed to follow an isotropic hyperelastic law. The polynomial form of the strain energy potential was chosen from the ABAQUS material library. Experimental data from Wagner and Lotz [42] were used. The nucleus was modeled as nearly incompressible, and its material properties were obtained from literature [33]. Material properties of ligaments were obtained from the Pintar et al. [25] study. Vertebral body,
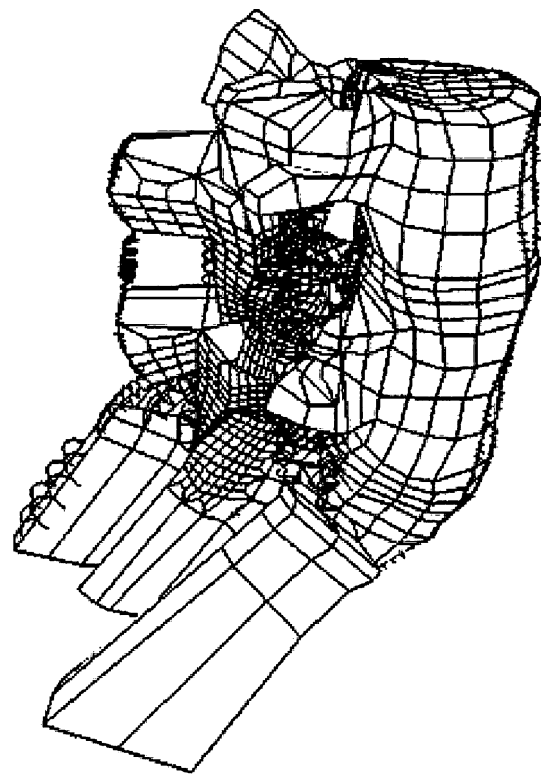

Fig. 1 Mesh of the L4–S1 finite element model

endplate, and posterior elements were assigned linear elastic material properties according to the literature [12, 33]. Element types and material properties used in the present model are listed in Table 1.

2.3 Boundary conditions and loads

All nodes on the inferior surface of S1 were constrained in all degrees-of-freedom. Nodes on top of the L4 vertebra were defined as coupling nodes. A reference node was created and connected to all coupling nodes. A coupling element was thus created to distribute moments on the reference node. Use of the coupling element eliminated the need to create additional rigid or other types of elements used in literature to apply moment loading [2, 18]. A pure moment of 4.0 Nm was applied to the coupling element so that the moment was distributed equally to all nodes. Flexion and extension and left and right lateral bending loading conditions were used. Numerical analyses were performed using ABAQUS version 6.4 (ABAQUS Inc., Providence, RI, USA). The nonlinearity control of the analyses allowed large deformations and simulation of contact behavior in the facet joints. Kinematic moment–rotation response of L4 with respect to L5 (monosegment), L5 with respect to S1 (monosegment), and L4 with respect to S1 (bisegment) were retrieved from the finite element simulation and compared with the entire range of experimental moment–rotation responses for validation.

2.4 Definition of response validation

The following definition was used for validating finite element model responses. All experimental data and numerical results were fitted into polynomial functions. Under each loading condition, the abscissa, i.e., moment, was evenly divided into 20 intervals, and corresponding rotation angles were obtained. The cumulative variance between the finite element model predicted response and experimental response was used to quantify the degree of validation. If the predicted response fell within the experimental corridor (mean ± 1 standard deviation), cumulative variance was set to zero, and the model was considered fully validated under the specific loading mode (Fig. 2). If the response did not fall completely within the corridor, the model was considered partially validated, and the cumulative variance was reported.

3 Results

A comparison of vertebral geometry, i.e., lateral width, anterior–posterior depth, transverse process width, spinous process length, and pedicle width and height with human cadaver data from literature is shown in Fig. 3. These data indicated that vertebral dimensions and height data from the model are representative of the adult population. Figure 4 shows moment–rotation responses under flexion and extension, and lateral bending modes for the bisegment L4–S1. Predicted flexion and extension responses were inside the experimental corridor (cumulative variance = 0). Left lateral bending results were very close to the lower bound of experimental data (cumulative variance = 2.6). Right lateral bending moment–rotation response fell within the experimental corridor beyond a moment level of 2.5 Nm, although at low load levels the response was outside the corridor. The cumulative

Table 1 Material properties and element types of the finite element model

| Component	Element type	No. of elements	Young's modulus E (Mpa)	Poisson ratio v
Cortical bone	4-Node shell	243	12,000	0.3
Endplate	4-Node shell	180	25	0.3
Cancellous bone	8-Node solid	495	100	0.2
Posterior elements	8-Node solid	2,606	3,500	0.25
Nucleus pulposus	8-Node solid	144	1.0	0.499
Annulus	8-Node solid	216	Hyperelastic material	Hyperelastic material
Ligaments	Spring	330	Stiffness (N/mm)-L4–5 level	Stiffness (N/mm)-L5–S1 level
Anterior longitudinal		76	40.5 ± 14.3	13.2 ± 10.2
Posterior longitudinal		114	25.8 ± 15.8	21.8 ± 16.0
Ligamentum flavum		40	27.2 ± 12.2	20.2 ± 8.4
Capsular		40	30.6 ± 1.5	29.9 ± 22.0
Interspinous		16	8.7 ± 6.5	16.3 ± 15.0
Supraspinous		20	18.0 ± 6.9	17.8 ± 3.8
Intertransverse		24	8.7 ± 6.5	16.3 ± 15.0
Facet joint	3D contact	560	–	–
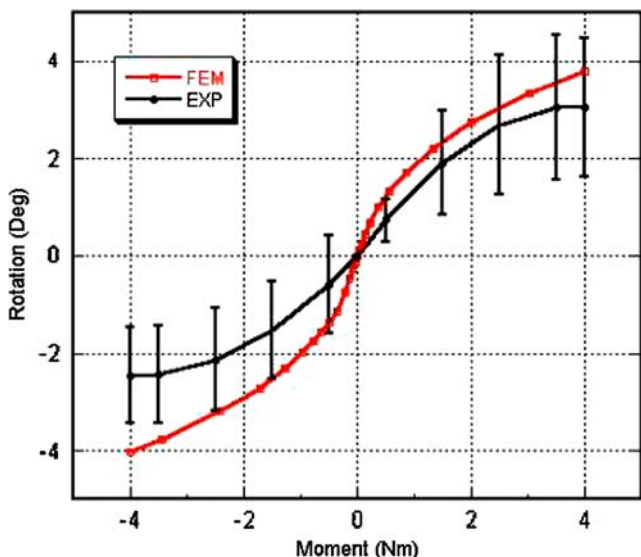
Fig. 2 Representative rotation–moment plot used for definition of curve validation

variance was 0.1. Figure 5 shows moment–rotation responses under flexion and extension and lateral bending modes for the monosegment L5–S1. Predicted extension response matched mean experimental data very well (cumulative variance = 0). Flexion response was inside the experimental corridor. Right lateral bending response also fell within the experimental corridor. Cumulative variances for these loadings were zero. A majority of left bending responses was inside the corridor except at low load levels. The cumulative variance was 0.1. Moment–rotation responses under flexion and extension and lateral bending modes for the monosegment L4–L5 is shown in Fig. 6. Predicted responses for both flexion and right lateral bending fell within the experimental corridor (cumulative variance = 0). However, predicted extension and left lateral bending results were outside the lower bound limit of the experimental corridor. Cumulative variance for extension and left lateral bending were 7.3 and 1.7.

All cumulative variance values are listed in Table 2. According to the definition of validation, the model
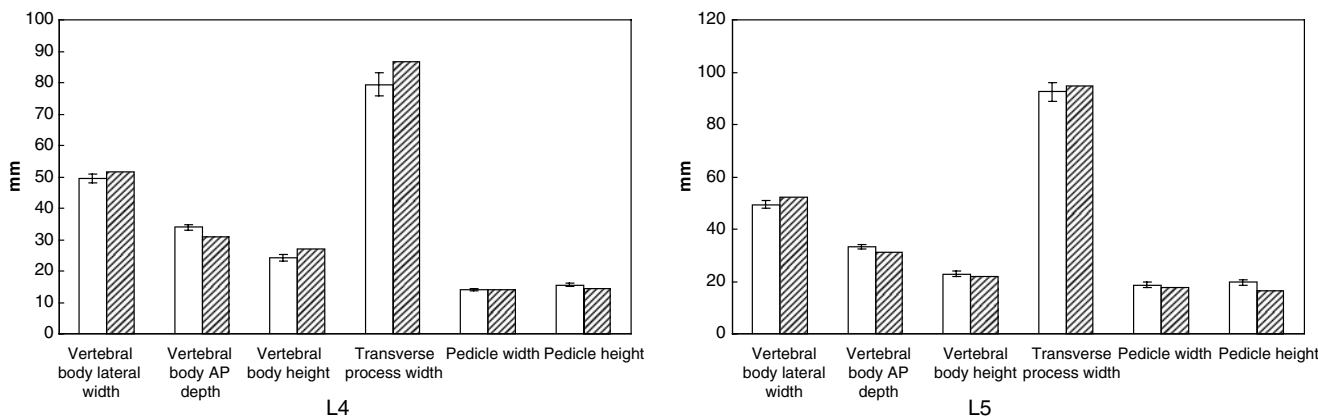

Fig. 3 Comparison of vertebral geometry from the present model (*shadow*) with human cadaver studies (Panjabi et al. 1992). Standard deviations are shown for experimental data

Fig. 4 Rotation–moment plots of flexion/extension and lateral bending for L4–S1
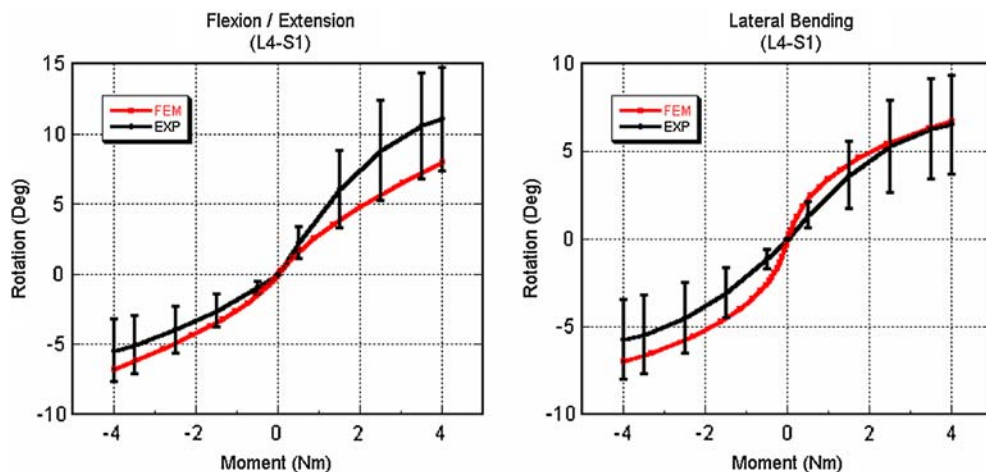
Fig. 5 Rotation–moment plots of flexion/extension and lateral bending for L5–S1
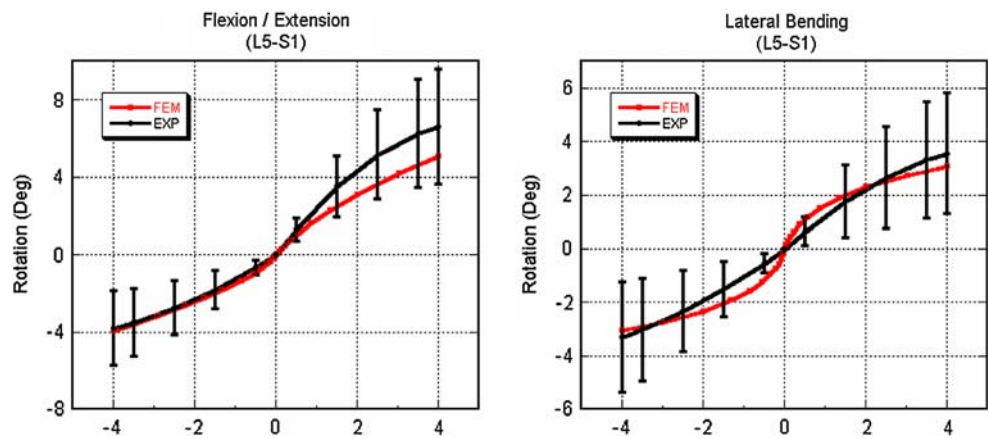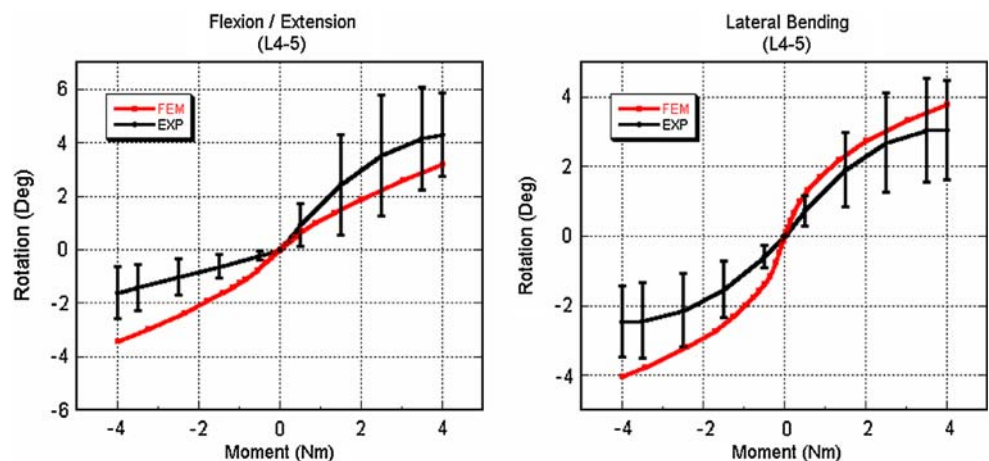

Fig. 6 Rotation–moment plots of flexion/extension and lateral bending for L4–5

was considered fully validated for both L4–S1 and L5–S1 segments under flexion and extension loading modes and right lateral bending for the L5–S1 segment. At the L4–L5 level, the model was fully validated for flexion and right lateral bending and partially validated for other modes. Figure 4 shows the response of two intervertebral L4–S1 segments, while Figs. 5 and 6 show responses from single intervertebral L4–L5 and L5–S1 segments. Deviations are likely due to the choice of level-specific material properties that were chosen from previous studies.

Table 2 Cumulative variance under different loading modes for different segment levels

Cumulative variance	L4–S1	L5–S1	L4–L5
Flexion	0.0	0.0	0.0
Extension	0.0	0.0	7.3
Right lateral bending	0.1	0.0	0.0
Left lateral bending	2.6	0.1	1.7

4 Discussion

Geometry, material properties, loading, and boundary conditions, followed by validation are the critical issues in finite element modeling of the spine [46, 48]. Advances in software and improvements in processing power have made it possible to use CT or magnetic resonance imaging technology to reconstruct three-dimensional models to capture the irregular bony structure of the spine [47, 49]. Using these techniques, high-quality finite element mesh can be developed for analysis. The present study used CT images to construct the geometry of lumbosacral spine.

4.1 Annulus fibrosus properties

The annulus fibrosus is nonlinear, heterogeneous, and anisotropic [9, 10]. Due to its important role in physiological loading, material modeling of this component has been widely studied using the finite element method. In [1], Belytschko et al. developed a finite element model of the lumbar intervertebral disc assuming axial symmetry with linear orthotropic

material properties. Kulak et al. [17] extended this model and assumed the annulus fibrosus to be non-linear and orthotropic. Since 1980s, two major methods have been used for disc modeling. In the *structural model*, fiber-induced anisotropy is represented by using tension-only cable or truss element embedded in an isotropic ground substance [12–14, 31, 33, 34]. In the *hyperelastic fiber-reinforced composite model*, the constitutive law is derived by combining structural tensors and invariant terms of the strain tensor into a strain energy function [5, 7, 8, 15, 42, 43]. The structural model requires fiber and matrix modulus, fiber and matrix Poisson's ratio, and fiber volume fraction. These properties are difficult to measure directly. Shirazi-Adl et al. [33] extracted matrix modulus from the initial portion of the stress–strain curves of the annulus and determined the collagen fiber modulus from its ultimate tensile strength. In the hyperelastic fiber-reinforced model, independent invariant terms (up to 11) are incorporated into a large number of permissible energy functions, polynomial or exponential. While these functions are appealing, the physical significance of the mathematical expression is not straightforward [45]. In addition, material parameters become non-unique when these constants are determined by fitting experimental outcomes [21].

In the present study, a simple and efficient approach was implemented to model the lumbosacral spine. The annulus fibrosis was modeled by an isotropic hyperelastic law without differentiating between the ground substance and fibers. Coefficients of the polynomial strain energy function were determined from experimental data [42]. As shown in Figs. 3 through 5 and cumulative variance values, this approach resulted in high-quality validation over the entire range in moment–rotation responses under four modes and for the different segments of the lumbosacral spine.

4.2 Loads

As one of the important features of finite element analysis, loading conditions must match between the model and experiment from which data are derived. In Shirazi-Adl et al. [34] and Goel et al. [12] studies, sagittal plane flexion and extension bending was represented by linearly varying axial loads acting at the top of the upper vertebra. In Natarajan et al. [20] and Chosa et al. [3] studies, flexion and extension moments were generated by applying a pair of equal and opposite axial forces at the anterior and posterior ends on the top surface of the L4 vertebral body. Posterior elements were not included in the loading process. This approach may induce stress concentration and not

replicate the actual condition wherein the entire upper vertebra was reported to be embedded in Polymethylmethacrylate in experimental studies to compare finite element model rotation at a single at single moment value of 10 Nm [20]. Charriere et al. [2] improved the loading technique in their finite element model by using rigid beam elements attached to the endplate of the superior surface of the L5 vertebrae. These beam elements were concentrated to a single node, where a pure torque was applied to follow the motion of L5. In the present study, a distributing coupling element was used to couple all nodes on the rostral surface of L4 through a reference node. The moment was distributed such that the force resultants on the coupling nodes (rostral surface of L4) were equal to the forces and moments on the coupling element node. This method accurately mimicked the mechanical loading used in experiments.

4.3 Experimental data for validation

The quality of the validation process of finite element models depends on the type of selected experimental data. Most finite element models have been validated by comparing predicted data with experimental studies [22, 29, 36]. In the Schultz et al. [29] study, mechanical behavior of 42 cadaver lumbar motion segments were obtained under flexion, extension, lateral bending, and torsion. Average motion results were reported from 11 L1–L2 segments, 8 L2–L3 segments, 13 L3–L4 segments, and 10 L4–L5 segments. In the Panjabi et al. [22] study, motion data were averaged from eight functional spinal units consisting of one T12–L1, one L2–L3, three L3–L4, and three L4–L5 segments. Tencer et al. [36] reported average mechanical properties of disc from eight L2–L3 and eight L4–L5 segments. Average range of motion data retrieved from the above experimental studies were grouped, albeit from different lumbar spine levels. This approach ignores response variations between spinal levels. The finite element model of the L2–L3 segment in the Shirazi-Adl et al. [34] study was validated with data obtained from the Schultz et al. [29] and Tencer et al. [36] experiments. Goel et al. [12] validated L4–L5 model with data from the Schultz et al. [29] study. The finite element model of the L2–L3 segment in the Teo et al. [38] study was validated with data from Panjabi et al. [22] experiments. It should be noted that researchers have published entire moment–rotation curves under different loading modes. While full experimental response curves are available, finite element models appear to be selective in choosing specific test data for establishing validity of the stress analysis

output. This selection process may dampen the confidence in model predictions, particularly with regard to intrinsic variables such as strain/stress in spinal components and clinical applicability.

4.4 Validation process

As indicated, most lumbar spine finite element models have been validated under single specific moment amplitude. Although finite element models were nonlinear, the predicted rotation was matched at one moment value in Shirazi-Adl and Parnianpour [32], Shirazi-Adl [31], and Natarajan et al. [20] studies. This approach ignores the nonlinear behavior identified in the experimental moment–rotation responses. From this perspective, these earlier attempts to understand the biomechanics of the lumbosacral spine can be considered as a primary step. Some models [34, 39] have compared numerical results with entire experimental curves. However, because the range of numerical prediction was beyond experimental data, the fidelity of the validation may be sacrificed. Model predictions have more confidence if responses are validated over the entire range. In the Eberlein et al. [6] study, numerical results of the L2–S1 model under extension and axial torsion loads showed good agreement with experimental data in the entire range but not under flexion and lateral bending modes. This study did not quantify the level or degree of validation, a process used in the present study. Furthermore, unlike cervical spine experiments wherein strain data on vertebral body and facet joint have been measured under different loading conditions [26], in the lumbosacral spine, moment–rotation curves appear to be the only response finite element modelers have used for validation. Therefore, it is critical to match these curves as closely as possible during the validation process.

In the present study, moment–rotation responses were computed using the finite element model under flexion and extension and left and right lateral bending and were validated with experiments. The same range of loading applied in the experiment was used for validating the finite element model outputs. Nonlinearities in the mechanical behavior were quantitatively evaluated using the cumulative variance parameter. All moment–rotation curves were considered to be fully validated except in three cases, left lateral bending for the L4–S1 and L4–L5 segments and extension for the L4–L5 segment (Table 2). The exact reason for this relatively discrepancy may be due to factors such as anisotropy, inhomogeneity, simplification of the complex behavior of spinal components, etc. However, to our best knowledge, this is the first study that has

attempted and provided quantified validation information for finite element modeling under different modes and to both segments of the lower lumbar and sacral spine. With this qualification and level of validation over the entire range moment–rotation responses, stress analysis output simulating clinical situations (e.g., cage instrumentation) can be obtained and interpreted with increased level of confidence. The present model performs better than previous models because it has been validated in the entire nonlinear range of the moment–rotation response instead of validating at a specific data point, a method often used in previous finite element models. In addition, the model used level-specific material properties and anatomically accurate geometry by including various components of the lumbosacral spinal structure. However, since the model is only validated using quasi-static loads, in order to delineate dynamic responses, data from dynamic tests including rate-dependent material properties are needed before the output of stress analysis can be applied to clinical situations.

The practical impetus for the present modeling effort lies in the lack of standardized and quantitatively validated models of the lumbosacral spine. In clinical situations, disorders of the lumbar spine overwhelmingly favor locations modeled in the present study. Unfortunately, clinical literature is replete with Class III data advocating the employment of procedures in this region that are eventually shown to be ineffective and subsequently abandoned. Clinical intuition, cadaver studies, and animal studies, while invaluable, often fail to predict the ultimate success or failure of a given intervention in a patient. The approach demonstrated in this model has the unique potential to assist health care providers by providing information on normal and degenerated spines. Data regarding mechanisms of internal load transfer and stresses and strains in the intervertebral components might assist in making predictions about spinal stability.

References

1. Belytschko T, Kulak R, Schultz A (1974) Finite element stress analysis of an intervetebral disc. J Biomech 7:277–285
2. Charriere E, Sirey F, Zysset P (2003) A finite element model of the L5–S1 functional spinal unit: development and comparison with biomechanical tests in vitro. Comput Methods Biomech Biomech Eng 6:249–261
3. Chosa E, Totoribe K, Tajima N (2004) A biomechanical study of lumbar spondylolysis based on a three-dimensional finite element method. J Orthop Res 22:158–163

4. Decker H, Shapiro S (1957) Herniated lumbar intervertebral disks; results of surgical treatment without the routine use of spinal fusion. AMA Arch Surg 5:77–84

5. Eberlein R, Holzapfel G, Schulze-Baur C (2001) An aniso-tropic constitutive model for annulus tissue and enhanced finite element analyses of intact lumbar disc bodies. Comput Meth Biomech Biomed Eng 4:209–230

6. Eberlein R, Holzapfel G, Frohlich M (2004) Mutli-segment FEA of the human lumbar spine including the heterogeneity of the annulus fibrosus. Comput Mech 4:147–163

7. Elliott D, Setton L (2000) A linear material model for fiber induced anisotropy of the annulus fibrosus. J Biomech Eng 122:173–179

8. Elliott D, Setton L (2001) Anisotropic and inhomogenous tensile behavior of the human annulus fibrosus: experimental measurement and material model predictions. J Biomech Eng 123:256–263

9. Farfan (1973) Mechanical disorder of the low back. Lea & Febiger, Philadelphia

10. Galante JO (1967) Tensile properties of the human lumbar anulus fibrosus. Acta Orthop Scand Suppl 100:1–91

11. Goel VK, Goyal S, Clark C, Nishiyama K, Nye T (1985) Kinematics of the whole lumbar spine-effect of discectomy. Spine 10:543–554

12. Goel VK, Kim YE, Lim TH, Weinstein JN (1988) An ana-lytical investigation of the mechanics of spinal instrumenta-tion. Spine 13:1003–1011

13. Goel VK, Kong WZ., Han JS, Weinstein JN, Gilbertson LG (1993) A combined finite element and optimization investi-gation of lumbar spine mechanics with and without muscles. Spine 18:1531–1541

14. Goel VK, Monroe BT, Gilbertson LG, Brinckmann P (1995) Interlaminar shear stresses and laminae separation in a disc: finite element analysis of the L3–4 motion segment subjected to axial compressive loads. Spine 20:689–698

15. Klisch S, Lotz J (1999) Application of a fiber-reinforced continuum theory to multiple deformations of the annulus fibrosus. J Biomech 32:1027–1036

16. Kortelainen P, Puranen J, Koivisto E, Lahde S (1985) Symptoms and signs of sciatica and their relation to the localization of the lumbar disc herniation. Spine 10:88–92

17. Kulak R, Belytschko T, Schultz A, Galante J (1976) Non-linear behavior of the human intervertebral disc under axial load. J Biomech 9:377–386

18. Kumaresan S, Yoganandan N, Pintar FA, Maiman DJ, Ku-ppa S (2000) Biomechanical study of pediatric human cer-vical spine: a finite element approach. J Biomech Eng 122:60–71

19. Natarajan R, Andersson G, Patwardhan A, Andriacchi T (1999) Study on effect of graded facetectomy on change in lumbar motion segment torsional flexibility using three-dimensional continuum contact representation for facet joints. J Biomech Eng 121:215–221

20. Natarajan R, Garretson R, Buyani A, Lim T, Andersson G, Howard A (2003) Effects of slip severity and loading direc-tions on the stability of isthmic spondylolisthesis. Spine 28:1103–1112

21. Ogden R, Saccomandi G, Sgura I (2004) Fitting hyperelastic models to experimental data. Comput Mech 34:484–502

22. Panjabi M, Krag MH, Chung TQ (1984) Effects of disc injury on mechanical behavior of the human spine. Spine 9:707–713

23. Panjabi M, Yamamoto I, Oxland T, Crisco J (1989) How does posture affect coupling in the lumbar spine? Spine 14:1002–1011

24. Panjabi M, Oxland T, Yamamoto I, Crisco J (1994) Mechanical behavior of the human lumbar and lumbosacral spine as shown by three-dimensional load-displacement curves. J Bone Joint Surg 76A:413–423

25. Pintar FA, Yoganandan N, Myers T, Elhagediab A, Sances A Jr (1992) Biomechanical properties of human lumbar spine ligaments. J Biomech 25:1351–1356

26. Pintar FA, Yoganandan N, Pesigan M, Reinartz JM, Sances A Jr, Cusick JF (1995) Cervical vertebral strain measure-ments under axial and eccentric loading. J Biomech Eng 117:474–478

27. Polikeit A, Nolte LP, Ferguson SJ (2003) The effect of ce-ment augmentation on the load transfer in an osteoporotic functional spinal unit: finite-element analysis. Spine 28:991–996

28. Polikeit A, Nolte LP, Ferguson SJ (2004) Simulated influ-ence of osteoporosis and disc degeneration on the load transfer in a lumbar functional spinal unit. J Biomech 37:1061–1069

29. Schultz A, Warwick D, Berkson M, Nachemson A (1979) Mechanical behavior of human lumbar spine motion seg-ments—Part I. Responses in flexion, extension, lateral bending and torsion. J Biomech Eng 101:46–52

30. Sharma M, Langrana NA, Rodriguez J (1995) Role of liga-ments and facets in lumbar spinal stability. Spine 20:887–900

31. Shirazi-Adl SA (1994) Biomechanics of the lumbar spine in sagittal/lateral moments. Spine 19:2407–2414

32. Shirazi-Adl A, Parnianpour M (1993) Nonlinear response analysis of the human ligamentous lumbar spine in com-pression. On mechanisms affecting the postural stability. Spine 18:147–158

33. Shirazi-Adl SA, Shrivastava SC, Ahmed AM (1984) Stress analysis of the lumbar disc-body unit in compression, a three-dimensional nonlinear finite element study. Spine 9:120–134

34. Shirazi-Adl SA, Ahmed AM, Shrivastava SC (1986) A finite element study of a lumbar motion segment subjected to pure sagittal plane moments. J Biomech 19:331–350

35. Spangfort E (1972) The lumbar disc herniation. A computer-aided analysis of 2504 operations. Acta Orthop Scand 142:40–44

36. Tencer A, Ahmed A, Burke D (1982) Some static mechan-ical properties of the lumbar intervertebral joint, intact and injured. J Biomech Eng 104:193–201

37. Teo E, Lee K, Ng H, Qiu T, Yang K (2003) Determination of load transmission and contact force at facet joints of L2–3 motion segment using FE method. J Musculoskeltal Res 7:97–109

38. Teo E, Lee K, Qiu T, Ng H, Yang K (2004) The biome-chanics of lumbar graded facetectomy under anterior-shear load. IEEE Trans Biomed Eng 51:443–449

39. Totoribe K, Tajima N, Chosa E (1999) A biomechanical study of posterolateral lumbar fusion using a three-dimen-sional nonlinear finite element method. J Orthop Sci 4:115–126

40. Totoribe K, Chosa E, Tajima N (2004) A biomechanical study of lumbar fusion based on a three-dimensional non-linear finite element method. J Spinal Dis Tech 17:47–153

41. Ueno K, Liu YK (1987) A three-dimensional nonlinear finite element model of lumbar intervertebral joint in torsion. Biomech Eng 109:200–209

42. Wagner D, Lotz J (2004) Theoretical model and experi-mental results for the nonlinear elastic behavior of human annulus fibrosus. J Orthop Res 22:901–909

43. Wu HC, Yao RF (1976) Mechanical behavior of the human anulus fibrosus. J Biomech 9:1–7

44. Yamamoto I, Panjabi M, Crisco T, Oxland T (1989) Three dimensional movements of the whole lumbar spine and lumbosacral joint. Spine 14:1256–1260

45. Yin L, Elliott D (2004) A homogenization model of the annulus fibrosus. J Biomech 37:907–916

46. Yoganandan N, Myklebust JB, Ray G, Sances A Jr (1987) Mathematical and finite element analysis of spinal injuries. CRC Rev Biomed Eng 15:29–93

47. Yoganandan N, Kumaresan S, Voo L, Pintar F (1996) Finite element applications in human cervical spine modeling. Spine 21:1824–1834

48. Yoganandan N, Kumaresan S, Voo L, Pintar FA (1997) Finite element model of the human lower cervical spine: parametric analysis of the C4–C6 unit. J Biomech Eng 119:87–92

49. Yoganandan N, Kumaresan S, Pintar FA (2001) Biomechanics of the cervical spine. Part 2. Cervical spine soft tissue responses and biomechanical modeling. Clin Biomech 16:1–27

50. Zander T, Rohlmanm A, Calisse J, Bergmann G (2001) Estimation of muscle forces in the lumbar spine during upper-body inclination. Clin Biomech 16:S73–S80

51. Zander T, Rohlmanm A, Bergmann G (2004) Influence of ligament stiffness on the mechanical behavior of a functional spinal unit. J Biomech 37:1107–1111